Proceedings of The 2019 IEEE International
Conference on Real-time Computing and Robotics
August 4-9, 2019, Irkutsk, Russia

Mobility Characteristics Analysis of a Dual-Continuum-Joint Translator

Lingyun Zeng, Xu Liu, Yang Zheng and Kai Xu*, *Member*, *IEEE*

***Abstract*— A design library of continuum mechanisms, which consists of various mechanism modules with different motion characteristics, can greatly facilitate design tasks. A recent addition to this design library is a dual-continuum-joint translator. This translator is composed of two continuum joints and a multi-lumen tube. The two continuum joints are identical in size and coupled by connecting their corresponding backbones inside the multi-lumen tube. This translator was previously used in constructing a continuum delta robot with a parallel structure and three translation DoFs (Degrees of Freedom). Even though the validity of the dual-continuum-joint translator was experimentally demonstrated, a theoretical characterization is still missing. This paper hence presents a mobility characteristics analysis of the dual-continuum-joint translator. Cosserat rod theory and screw theory are used to analyze the mobility characteristics of this translator. First, the deflected shapes and the compliance matrices of the translator are calculated using Cosserat rod theory. Then, the mobility characteristics of the translator is investigated using screw theory by quantifying the primary mobility. Results of the calculated deflected shapes show that under external wrenches exerted on the translator, the two coupled continuum joints have the bending shapes close to circular curves with similar bending angles. The calculated compliance matrices indicate that translation is the translator's primary mobility.**

I. Introduction

Continuum robots have attracted extensive attentions due to various advantages, such as safe interaction with environment, motion dexterity and design compactness [1]. Motions of continuum robots rely on deformation of their flexible members which can be springs [2], flexures [3] or flexible beams [4]. Continuum robots have found a variety of applications in medicine [5], inspection [6, 7] and manipulation [8-10].

A recent development in continuum robots is the proposal of Parallel Continuum Robot (PCR) [11]. A PCR usually consists of multiple elastic rods as its legs and generates multi-DoF (Degree of Freedom) movements through coordinated deflections of its legs. As a PCR's motion control intensively relies on complicated mechanics formulations, a new type of parallel-structured robot with continuum joints is proposed for simpler kinematics as in [12]. The proposed robot has a function similar to a Delta robot and is referred to as the Continuum Delta Robot (CDR), as shown in Fig. 1(a).

The CDR consists of three legs. Each leg includes i) two continuum joints that are coupled and identical in size, and ii) a multi-lumen tube. The two continuum joints are designated as the Proximal Joint (PJ) and the Distal Joint (DJ), as in Fig. 1(b). Each leg is then in fact a dual-continuum-joint translator.

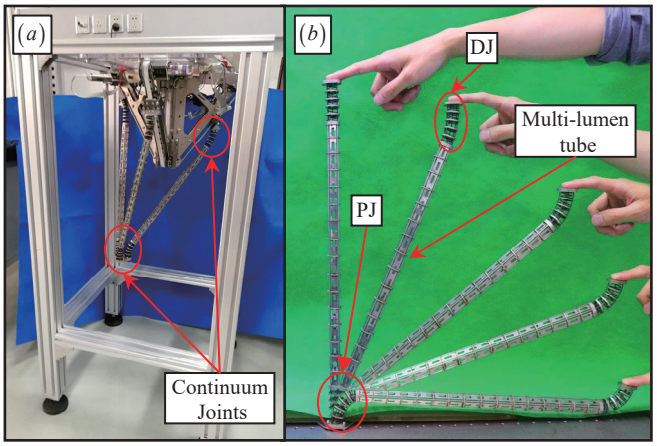

Fig. 1. Dual-continuum-joint translator: (a) used in a Continuum Delta Robot with three such translators, and (b) shapes of one such translator.

Even though the validity of the dual-continuum-joint translator was experimentally demonstrated in [12], a theoretical characterization is yet to be investigated. Thus, this paper examines the mobility characteristics of this dual-continuum-joint translator. Since the flexible backbones of the continuum joint undergo deformations along their total lengths under external wrenches, the deformed patterns will be characterized by primary and parasite motions.

The primary mobility can be quantified by calculating the compliance matrix of a compliant manipulator as in [13]. Cosserat rod theory is used here to establish the kinestatic model, according to its recently demonstrated effectiveness [11, 14]. The compliance matrix is then computed through a finite difference approach referring to [15] for the quantification of the primary mobility of the translator.

This paper is organized as follows. Section II describes the structure of the translator, while Section III presents the kinestatic modeling. Mobility characteristics are analyzed in Section IV with the conclusions summarized in Section V.

II. Description of the Translator

The dual-continuum-joint translator is used as one of the three legs of a CDR. It consists of two coupled continuum joints and a multi-lumen tube, as shown in Fig.1 (b) and Fig. 2.

This work was supported in part by the National Natural Science Foundation of China (Grant No. 51722507, Grant No. 51435010 and Grant No. 91648103), and in part by the National Key R&D Program of China (Grant No. 2017YFC0110800).

Lingyun Zeng, Xu Liu, Yang Zheng and Kai Xu are with School of Mechanical Engineering, Shanghai Jiao Tong University, Shanghai, China (asterisk indicates the corresponding author, phone: 86-21-34206547; emails: me_maxqi@sjtu.edu.cn, xu.liu@sjtu.edu.cn, zzyy0608@sjtu.edu.cn, and k.xu@sjtu.edu.cn).

978-1-7281-3726-1/19/$31.00 © 2018 IEEE

Each continuum joint consists of an end disk, a few spacer disks and several super-elastic nitinol backbones.

The backbones include four secondary ones and a central primary one, as shown in Fig. 2. The four equidistantly arranged secondary backbones are clamped at the end disks and can slide freely in the holes of the spacer disks and inside the multi-lumen tube. The primary backbone is attached to all the disks and the multi-lumen tube and located centrally to maintain the equal spacing of the spacer disks.

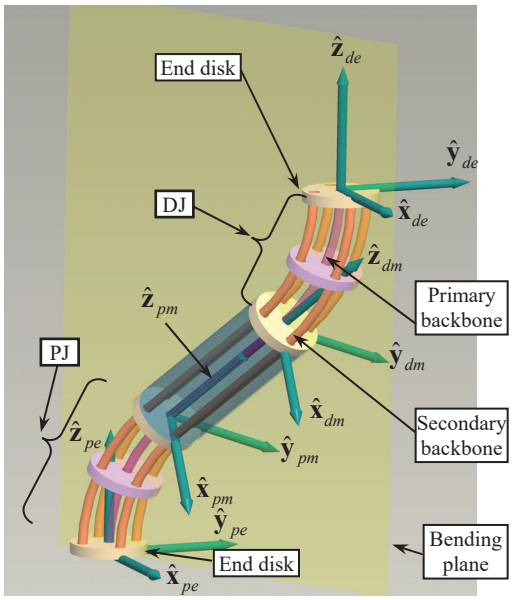

Fig. 2. Nomenclature and coordinates of the dual-continuum-joint translator

The two continuum joints are identical in size and their corresponding backbones are connected as one piece through the multi-lumen tube. When the end disk of the proximal joint (PJ) is fixed to a base and an external wrench is exerted on the end disk of the distal joint (DJ), the coupled PJ and DJ will bend passively for a similar amount. Hence, The DJ's end disk of the translator produces translational movements through the coupling between the PJ and the DJ. In the experimentally verified motion patterns [12], the translational movements are along two directions, one is along the direction which is perpendicular to the bending plane, the other direction is within the bending plane.

III. Kinestatic Modeling

In this section, a kinestatic model is derived for the translator. The modeling approach is based on the Cosserat rod theory and the translator is modeled as a set of Cosserat rods subject to multiple boundary conditions associated with the spacer disks and the end disks of the translator.

In the kinestatic model, the number of the spacer disks is reduced to 2 in order to simplify the calculation without loss of generality. The primary backbone is located centrally and clamped to all disks and the multi-lumen tube to keep the equal spacing between the spacer disks.

The Cosserat rod theory is briefly presented in Section III.B. Then the boundary conditions are applied to these equations to form a boundary value problem as in Section III.C. A numerical solution implementation is proposed to solve these equations as in Section III.D. Similar approach was also adopted in [16].

A. Nomenclature and Coordinates

Four coordinate systems are attached to the translator, referring to Fig. 2. Nomenclature is defined in Table I.

- *PJ End Disk Coordinate* $\{pe\} \equiv \{\hat{\mathbf{x}}_{pe}, \hat{\mathbf{y}}_{pe}, \hat{\mathbf{z}}_{pe}\}$ is attached to the center of the end disk of the PJ.
- *Proximal Tube Coordinate* $\{pm\} \equiv \{\hat{\mathbf{x}}_{pm}, \hat{\mathbf{y}}_{pm}, \hat{\mathbf{z}}_{pm}\}$ is fixed to the center of the multi-lumen tube's proximal end.
- *Distal Tube Coordinate* $\{dm\} \equiv \{\hat{\mathbf{x}}_{dm}, \hat{\mathbf{y}}_{dm}, \hat{\mathbf{z}}_{dm}\}$ is attached to the center of the multi-lumen tube's distal end.
- *DJ End Disk Coordinate* $\{de\} \equiv \{\hat{\mathbf{x}}_{de}, \hat{\mathbf{y}}_{de}, \hat{\mathbf{z}}_{de}\}$ is attached to the center of the end disk of the DJ.

TABLE I. Nomenclature Used in This Paper

Symbol	Definition
i	Index of the backbones, i = 1, 2, 3, 4 designates the four secondary backbones that can slide freely in the holes of the spacer disks; and i = 0 designates the primary backbone.
j	Index of the disks, j = 1,3 designates the two spacer disks; j = 2 designates the multi-lumen tube, which is regarded as a spacer disk with a length L_m; and j = 4 designates the end disk of the DJ.
$\mathbf{r}_{i,j}$	$\mathbf{r}_{i,j}$ represents the constraint hole's location in the j^{th} disk through which the i^{th} backbone pass.
L_i	L_i is the total length of the i^{th} backbone.
r	r is the radius of the pitch circle along which the four secondary backbones are arranged; r =10 mm is a constant.
d_i	d_i is the diameter of the i^{th} backbone; d_i = 1.2 mm is a constant.
D	D is the distance between two adjacent spacer disks of each continuum joint; D = 10 mm is a constant.

B. Cosserat Rod Equations for a Single Rod

Each elastic backbone of the dual-continuum-joint translator is modeled as a Cosserat rod. In Cosserat rod theory [17], a material frame $\mathbf{T}_i(s_i)$ can be attached to the cross section of the backbone i to describe the overall shape of the backbone.

$$\mathbf{T}_i(s_i) = \begin{bmatrix} \mathbf{R}_i(s_i) & \mathbf{p}_i(s_i) \\ \mathbf{0} & 1 \end{bmatrix} \tag{1}$$

Where s_i is the length along the backbone i, $\mathbf{p}_i(s_i) \in \mathbb{R}^3$ is the position of the backbone's centerline and $\mathbf{R}_i(s_i) \in$ SO(3) is the orientation of its cross section.

The derivative of $\mathbf{T}_i(s_i)$ with respect to s_i is written as:

$$\begin{aligned} \frac{d\mathbf{p}_i(s_i)}{ds_i} &= \mathbf{R}_i(s_i)\mathbf{v}_i(s_i) \\ \frac{d\mathbf{R}_i(s_i)}{ds_i} &= \mathbf{R}_i(s_i)[\mathbf{u}_i(s_i)\times] \end{aligned} \tag{2}$$

Where $\mathbf{v}_i(s_i)$ and $\mathbf{u}_i(s_i)$ represent the rates of change of $\mathbf{p}_i(s_i)$ and $\mathbf{R}_i(s_i)$ described in $\mathbf{T}_i(s_i)$, respectively; and $[\mathbf{p}\times]$ is the skew-symmetric matrix of vector $\mathbf{p}$.

The derivatives of the inner force $\mathbf{n}_i(s_i)$ and moment $\mathbf{m}_i(s_i)$ with respect to the backbone length s_i along the backbone's central line can be described via the static equilibrium equations:

$$\begin{aligned}\frac{d\mathbf{n}_i(s_i)}{ds_i} &= -\mathbf{f}_i(s_i)\\ \frac{d\mathbf{m}_i(s_i)}{ds_i} &= -\mathbf{l}_i(s_i) - \frac{d\mathbf{p}_i(s_i)}{ds_i}\times\mathbf{n}_i(s_i)\end{aligned} \tag{3}$$

Where $\mathbf{f}_i(s_i)$ and $\mathbf{l}_i(s_i)$ are the external forces and moments that are distributed on the backbone, respectively.

Following the constitutive law, $\mathbf{n}_i(s_i)$ and $\mathbf{m}_i(s_i)$ are related to the linear and angular rates of change of $\mathbf{T}_i(s_i)$, namely $\mathbf{v}_i(s_i)$ and $\mathbf{u}_i(s_i)$. In this paper, a linear constitutive law is used:

$$\begin{aligned}\mathbf{n}_i(s_i) &= \mathbf{R}_i(s_i)\mathbf{K}_{se,i}(\mathbf{v}_i(s_i) - \mathbf{v}_i^*(s_i))\\ \mathbf{m}_i(s_i) &= \mathbf{R}_i(s_i)\mathbf{K}_{bt,i}(\mathbf{u}_i(s_i) - \mathbf{u}_i^*(s_i))\end{aligned} \tag{4}$$

Where $\mathbf{v}_i^*(s_i)$ and $\mathbf{u}_i^*(s_i)$ is the reference rates of change of $\mathbf{T}_i(s_i)$ under the initial setting. In this dual-continuum-joint translator, the backbones are straight in its initially stress free state. Hence $\mathbf{v}_i^*(s_i) = [0\ 0\ 1]^T$ and $\mathbf{u}_i^*(s_i) = [0\ 0\ 0]^T$, the shear/extension stiffness matrices $\mathbf{K}_{se,i}$ and bending/torsion stiffness matrices $\mathbf{K}_{bt,i}$ are:

$$\begin{aligned}\mathbf{K}_{se,i} &= \mathrm{diag}(A_iG_i, A_iG_i, A_iE_i)\\ \mathbf{K}_{bt,i} &= \mathrm{diag}(I_iE_i, I_iE_i, J_iG_i)\end{aligned} \tag{5}$$

Where A_i is the area of the cross section; E_i is the material's Young's modulus; G_i is the material's shear modulus; I_i is the second area moment of the cross section about the local x and y axes; and J_i is the polar area moment of the cross section about the local z axis.

Finally, a set of nonlinear ordinary differential equations can be obtained, combining Eq. (2) to Eq. (5):

$$\begin{aligned}&\frac{d\mathbf{p}_i(s_i)}{ds_i} = \mathbf{R}_i(s_i)\mathbf{v}_i(s_i),\ \mathbf{v}_i(s_i) = \mathbf{K}_{se,i}^{-1}\mathbf{R}_i^T(s_i)\mathbf{n}_i(s_i) + \mathbf{v}_i^*(s_i)\\ &\frac{d\mathbf{R}_i(s_i)}{ds_i} = \mathbf{R}_i(s_i)[\mathbf{u}_i(s_i)\times],\ \mathbf{u}_i(s_i) = \mathbf{K}_{bt,i}^{-1}\mathbf{R}_i^T(s_i)\mathbf{m}_i(s_i) + \mathbf{u}_i^*(s_i)\\ &\frac{d\mathbf{n}_i(s_i)}{ds_i} = -\mathbf{f}_i(s_i)\\ &\frac{d\mathbf{m}_i(s_i)}{ds_i} = -\mathbf{l}_i(s_i) - \frac{d\mathbf{p}_i(s_i)}{ds_i}\times\mathbf{n}_i(s_i)\end{aligned} \tag{6}$$

C. Boundary Conditions and Constraints

The shape, the internal forces and moments of a single backbone under external wrenches can be described using the nonlinear ordinary differential equations in Eq. (6). At the meantime, the translator consists of several spacer disks and end disks that apply constraints to the backbones. Therefore, the constraints from the spacer disks and the end disks should be modelled as the boundary conditions.

A few assumptions should be made to describe the constraints from the spacer disks. Referring to [16, 18], the spacer disks are modelled to be infinitely thin and the holes in the spacer disks are assumed frictionless. In this way, the backbones' internal forces and moments are equal in the direction perpendicular to the spacer disks, as the backbones enter or exit the holes of the spacer disks.

Since the secondary backbones can slide and rotate in the holes of the spacer disks, the positions and orientation about the z axis of the backbones' local reference frames cannot be constrained by the spacer disks. The position and orientation constraints for the spacer disks are hence given by:

$$\begin{aligned}&[\mathbf{R}_0^T(s_{0,j})(\mathbf{p}_i(s_{i,j}) - \mathbf{p}_0(s_{0,j}) - \mathbf{r}_{i,j})]|_{xy} = \mathbf{0},\ i = 1,\cdots,4\\ &[\log(\mathbf{R}_0^T(s_{0,j})\mathbf{R}_i(s_{i,j}))]^\vee|_{xy} = \mathbf{0},\ i = 1,\cdots,4\end{aligned} \tag{7}$$

Where $s_{i,j}$ is the i^{th} backbone length from the PJ's end disk to the intersection with the j^{th} spacer disk. As the i^{th} backbone (i = 1, 2, 3, 4) slides through the holes of the spacer disks, $s_{i,j}$ varies according to the deflected shape of the translator under different external wrenches; $[\log(\mathbf{R})]^\vee$ gives the angled rotation axis vector of the rotation matrix $\mathbf{R}$; $\mathbf{p}|_{xy}$ are the 1st and the 2nd elements in the vector $\mathbf{p}$.

At the backbone's intersection with the spacer disks, the backbone length satisfies the following equation.

$$[\mathbf{R}_0^T(s_{0,j})(\mathbf{p}_i(s_{i,j}) - \mathbf{p}_0(s_{0,j}) - \mathbf{r}_{i,j})]|_z = \mathbf{0},\ i = 1,\cdots,4 \tag{8}$$

The static equilibrium needs to be satisfied for each spacer disk. As the backbone enters and exits the holes in the spacer disks, the internal forces and moments are denoted by superscript (−) and (+), respectively. It is assumed that zero external forces and moments are exerted on the spacer disks. Then the static equilibrium gives:

$$\begin{aligned}&\mathbf{R}_0^T(s_{0,j})\sum_{i=0}^{4}[-\mathbf{n}_i^-(s_{i,j}) + \mathbf{n}_i^+(s_{i,j})]|_{x,y} = \mathbf{0}\\ &\sum_{i=0}^{4}\begin{bmatrix}\mathbf{p}_i(s_{i,j})\times(-\mathbf{n}_i^-(s_{i,j}) + \mathbf{n}_i^+(s_{i,j}))\\ +(-\mathbf{m}_i^-(s_{i,j}) + \mathbf{m}_i^+(s_{i,j}))\end{bmatrix} = \mathbf{0}\end{aligned} \tag{9}$$

The constraints stemmed from the end disk of the DJ are different from those from the spacer disks due to the fact that the backbones are clamped to the end disk. The position and orientation constraints at the end disk are as follows:

$$\begin{aligned}&[\mathbf{R}_0^T(L_0)(\mathbf{p}_i(L_i) - \mathbf{p}_0(L_i) - \mathbf{r}_{i,4})] = \mathbf{0},\ i = 1,\cdots,4\\ &[\log(\mathbf{R}_0^T(L_0)\mathbf{R}_i(L_i))]^\vee = \mathbf{0},\ i = 1,\cdots,4\end{aligned} \tag{10}$$

Where $\mathbf{r}_{i,4}$ is the clamping location of the i^{th} backbone in the end disk.

Then the static equilibrium for the end disk is as follows.

$$\begin{aligned}&-\sum_{i=0}^{4}\mathbf{n}_i^-(L_i) + \mathbf{F}_e = \mathbf{0}\\ &-\sum_{i=0}^{4}\begin{bmatrix}\mathbf{p}_i(L_i)\times\mathbf{n}_i^-(L_i)\\ +\mathbf{m}_i^-(L_i)\end{bmatrix} + \mathbf{p}_0(L_0)\times\mathbf{F}_e + \mathbf{M}_e = \mathbf{0}\end{aligned} \tag{11}$$

Where $\mathbf{F}_e$ and $\mathbf{M}_e$ are the external force and moment exerted on the end disk.

D. Numerical Solution Implementation

A boundary value problem is formed as a set of first-order ordinary differential equations as in Eq. (6) subject to multiple boundary conditions as in Eq. (7), Eq. (9), Eq. (10) and Eq.

(11). An implicit function can be written to describe this multi-elastic-rod system with multi-point boundary conditions:

$$\begin{aligned}\boldsymbol{\varepsilon} &= \mathrm{f}(\mathbf{u}) \\ &= \mathrm{f}(\mathbf{n}_i(s_{i,0}), \mathbf{m}_i(s_{i,0}), \mathbf{n}_i^+(s_{i,j}), \mathbf{m}_i^+(\mathrm{s}_{i,j}))\end{aligned} \tag{12}$$

Where ε is the residual error vector that includes the left sides of Eq. (7), Eq. (9), Eq. (10) and Eq. (11); **u** is the initial guess vector which includes the internal forces and moments at the PJ's end disk, as well as at the intersections between each backbone and the spacer disks; $i = 0, \cdots, 4$ and $j = 1, 2, 3$.

In order to solve the boundary value problem, a shooting method is adopted here as shown in Fig. 3. The initial guess **u** is first given. Then the differential equations in Eq. (6) are integrated for the primary backbone via a standard Runge-Kutta method. Next, Eq. (6) are also integrated for the secondary backbones towards the intersection points where the condition in Eq. (8) should be satisfied. Thus the lengths $s_{i,j}$ where the secondary backbones intersects with the spacer disks can be obtained.

It should be noted that due to the interactions between the backbones and the thin spacer disks, the internal forces and internal moments of the backbones can change discontinuously at the intersection points where the backbone lengths are $s_{i,j}$. Thus in the programing implementation, the integral process of all backbones is divided into several ranges, namely from the PJ's end disk to the 1^{st} spacer disk, then from the 1^{st} spacer disk to the multi-lumen tube, and finally from the last spacer disk to the DJ's end disk. With the integrated results of all backbones, the constraints in Eq. (7), Eq. (9), Eq. (10) and Eq. (11) can be evaluated at the intersect points and residual error vectors can be calculated.

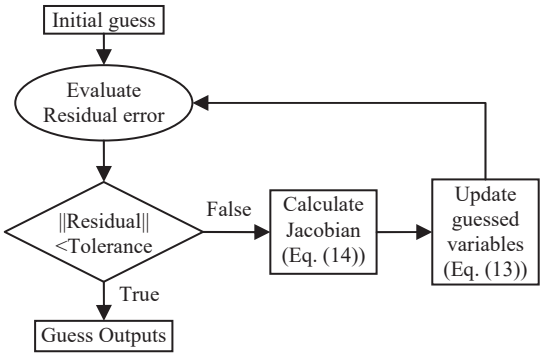

Fig. 3. Shooting method for solving the boundary value problem

After the residual error vector **ε** is calculated, using the following Levenberg-Marquardt formulation in Eq. (13), norm of the residual error will be iteratively reduced by updating the initial guess variables until norm of the error lesser than a specified tolerance value:

$$\mathbf{u}_{k+1} = \mathbf{u}_k + (\mathbf{J}_k^T \mathbf{J}_k + \lambda \mathbf{I})^{-1} \mathbf{J}_k^T \boldsymbol{\varepsilon}_k \tag{13}$$

Where k is the iteration index, λ is the damping parameter, **J** is the Jacobian matrix of the residual error vector with respect to the variables as in Eq. (14), a finite difference approach as in [14] was adopted to compute **J**.

$$\mathbf{J} = \partial \boldsymbol{\varepsilon} / \partial \mathbf{u} \tag{14}$$

In the solution process, the tolerances are 2×10^{-4} m, 1×10^{-4} rad, 1×10^{-4} N, and 1×10^{-4} Nm for the position, the orientation, force and moment equilibrium, the calculated residual error need to be satisfied within these tolerances at the same time.

IV. Mobility Characteristics of the Translator

Primary mobility of the dual-continuum-joint translator can be extracted from the calculated compliance matrices. With the compliance matrices, screw theory can be used to quantify the primary mobility.

In this section, the deflections of the translator under external wrenches exerted on the DJ's end disk are first calculated via the kinestatic model derived in Section III. Then the compliance matrices of the translator are calculated when its continuum joints are bent to different angles via a finite difference method. The eigenvalues and the eigenvectors of the compliance matrices are extracted to quantify the primary mobility of the translator.

A. Deflection under External Forces

When an external wrench is applied to the centroid of the DJ's end disk, the continuum joints would be bent and the translator would be deflected to generate a movement in its end disk. In this section, two simulation cases were studied where two different external forces were exerted on the translator.

Case study #1: $\mathbf{F}_e = [12\ \mathrm{N}\ 0\ 0]^T$, $\mathbf{M}_e = [0\ 0\ 0]^T$.

The deflected shapes of the translator are calculated when an external force $[12\ \mathrm{N}\ 0\ 0]^T$ is exerted, as shown in Fig. 4. The bent angles of the continuum joints (PJ and DJ) are listed in Table II. The bent angles are calculated from the rotation matrix of frame $\{pm\}$with respect to frame $\{pe\}$, and frame $\{de\}$ with respect to frame $\{dm\}$, respectively. The maximal position deviations between the calculated curve and the fitted circular curve of the backbones of the continuum joints (PJ and DJ) are also listed. It should be noted that the calculated curve is given as a set of discrete points so that the deviation calculation is based on the distances from the points to the fitted circle curve.

TABLE II. Deflection of The Translator

External force	$[12\ \mathrm{N}\ 0\ 0]^T$	$[20\ \mathrm{N}\ 0\ 0]^T$
Bending angle of PJ	22.448°	32.871°
Bending angle of DJ	22.063°	31.982°
Rotation angle of the end disk	0.385°	0.889°
Maximal position deviation from circular bending shapes	0.016 mm	0.012 mm

Case study #2: $\mathbf{F}_e = [20\ \mathrm{N}\ 0\ 0]^T$, $\mathbf{M}_e = [0\ 0\ 0]^T$.

The corresponding deflected shapes of the translator is shown in Fig. 4 as well. The bending angles of the PJ and the DJ, together with the maximal position deviations, are listed in Table II.

From the calculated deflected shapes of the translator, it can be seen that the end disk rotates a small angle (smaller than 0.889°). It is considered small enough compared to the bending

angles of the continuum joints. The output movements are hence close to translations. Furthermore, the maximal deviations between the calculated curves to the ideal circular curves are less than 0.016 mm. The bent shape of the continuum joints are close to circular arcs.

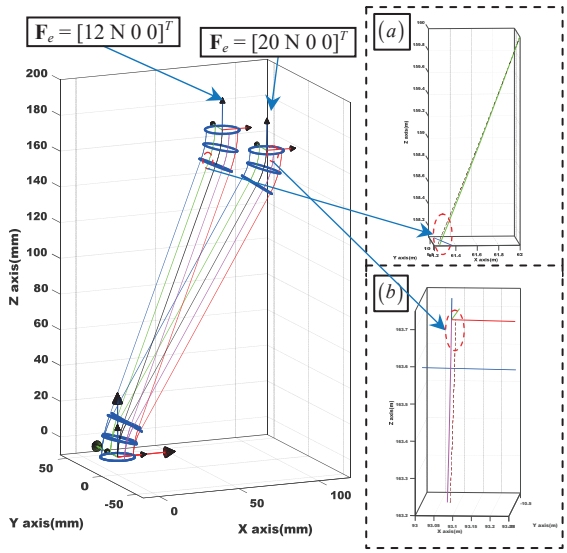

Fig. 4. Calculated deflected shapes (solid lines) and circular arcs (dashed lines) of the backbones of the translator under different external forces; enlarged side view for the maximum deviation under external force of (a) $[12\ \mathrm{N}\ 0\ 0]^T$ and (b) $[20\ \mathrm{N}\ 0\ 0]^T$.

B. *Compliance Matrices and Primary Mobility*

Compliance matrix $\mathbf{C}$ is a mapping from an external wrench to a twist as follows:

$$\begin{bmatrix} \mathbf{v} \\ \boldsymbol{\omega} \end{bmatrix} = \mathbf{C} \begin{bmatrix} \mathbf{f} \\ \mathbf{m} \end{bmatrix} \tag{15}$$

Where $\mathbf{v} \in \mathbb{R}^3$ and $\boldsymbol{\omega} \in \mathbb{R}^3$ are the linear and angular elements of a twist deformation, $\mathbf{f} \in \mathbb{R}^3$ and $\mathbf{m} \in \mathbb{R}^3$ are the force and moment of an external wrench.

The 6×6 compliance matrix $\mathbf{C}$ of the translator under external forces of $[12\ \mathrm{N}\ 0\ 0]^T$ and $[20\ \mathrm{N}\ 0\ 0]^T$ were both calculated via the kinestatic model and a finite difference process as detailed in [15]. In order to simply evaluate the primary mobility, the elements of the compliance matrix $\mathbf{C}$ that are close to zero are written as zeroes, as designated by $\mathbf{C}_s$. Each element of the vector $\boldsymbol{\xi}$ and each column vector of the matrix $\boldsymbol{\Gamma}$ are the eigenvalues and the corresponding eigenvectors of $\mathbf{C}_s$, respectively. The values of $\mathbf{C}$, $\mathbf{C}_s$, $\boldsymbol{\xi}$ and $\boldsymbol{\Gamma}$ in case study #1 and #2 are listed in Table III, respectively.

The primary mobility of the translator can be determined referring to the method proposed in [13]. As shown in Table III, the *red* column vectors of $\boldsymbol{\Gamma}$ span the constraint wrench space, while the *blue* column vectors of $\boldsymbol{\Gamma}$ are twists that indicate the primary mobility characteristics of the translator.

It should be noted that the primary mobility characteristics indicate a rotation, which is not intended output of the translator. However, this rotation mobility along the z axis is consistent with the observation that the joints can be twisted. Twisting resistant components should be arranged to minimize this possible twist so that the primary mobility of the translator is sole translation.

TABLE III. VALUES OF THE ENTITIES IN CASE STUDY #1 AND #2

Case Study 1 $\quad \mathbf{F}_e = [12\mathrm{N}\ 0\ 0]^T, \mathbf{M}_e = [0\ 0\ 0]^T$

$$\mathbf{C} = \begin{bmatrix} 0.0046 & -1.78\times10^{-6} & -0.0017 & -3.05\times10^{-5} & -8.68\times10^{-4} & -2.28\times10^{-4} \\ -6.41\times10^{-6} & 0.0053 & 6.77\times10^{-6} & 3.31\times10^{-5} & -7.98\times10^{-6} & -3.16\times10^{-4} \\ -0.0018 & -7.96\times10^{-6} & 6.72\times10^{-4} & 1.02\times10^{-5} & 3.37\times10^{-4} & 8.60\times10^{-5} \\ 4.53\times10^{-5} & 1.27\times10^{-4} & -4.84\times10^{-5} & 0.0093 & 6.04\times10^{-5} & 0.0077 \\ 2.30\times10^{-4} & -3.54\times10^{-5} & -6.45\times10^{-4} & -7.92\times10^{-4} & 0.0019 & -6.01\times10^{-4} \\ 3.38\times10^{-4} & -6.62\times10^{-4} & -4.12\times10^{-4} & 0.0112 & 5.11\times10^{-4} & 0.108 \end{bmatrix}$$

$$\mathbf{C}_s = \begin{bmatrix} 0.0046 & 0 & -0.0017 & 0 & 0 & 0 \\ 0 & 0.0053 & 0 & 0 & 0 & 0 \\ -0.0018 & 0 & 6.72\times10^{-4} & 0 & 0 & 0 \\ 0 & 0 & 0 & 0.0093 & 0 & 0.0077 \\ 0 & 0 & 0 & 0 & 0.0019 & 0 \\ 0 & 0 & 0 & 0.0112 & 0 & 0.1080 \end{bmatrix}$$

$$\boldsymbol{\xi} = \begin{bmatrix} 0.0053 & 5.9247\times10^{-6} & 0.0053 & 0.0084 & 0.1089 & 0.0019 \end{bmatrix}$$

$$\boldsymbol{\Gamma} = \begin{bmatrix} 0.9311 & 0.3470 & 0 & 0 & 0 & 0 \\ 0 & 0 & 1 & 0 & 0 & 0 \\ -0.3648 & 0.9378 & 0 & 0 & 0 & 0 \\ 0 & 0 & 0 & 0.9937 & 0.0771 & 0 \\ 0 & 0 & 0 & 0 & 0 & 1 \\ 0 & 0 & 0 & -0.1118 & 0.9970 & 0 \end{bmatrix}$$

Case Study 2 $\quad \mathbf{F}_e = [20\mathrm{N}\ 0\ 0]^T, \mathbf{M}_e = [0\ 0\ 0]^T$

$$\mathbf{C} = \begin{bmatrix} 0.0016 & 8.22\times10^{-4} & -0.001 & -4.05\times10^{-4} & 2.80\times10^{-4} & -5.28\times10^{-4} \\ -1.05\times10^{-5} & 0.0047 & 3.16\times10^{-5} & -6.55\times10^{-4} & 1.38\times10^{-4} & -2.06\times10^{-4} \\ -0.001 & -4.29\times10^{-4} & 6.54\times10^{-4} & 7.42\times10^{-4} & -1.39\times10^{-4} & 3.50\times10^{-5} \\ -1.49\times10^{-6} & -8.88\times10^{-6} & 8.47\times10^{-7} & 0.0130 & -6.04\times10^{-5} & 0.0095 \\ 6.61\times10^{-6} & 6.12\times10^{-5} & -4.05\times10^{-6} & -1.20\times10^{-4} & 0.0015 & -5.63\times10^{-4} \\ -6.36\times10^{-6} & 4.06\times10^{-7} & 4.38\times10^{-6} & 0.0083 & -1.05\times10^{-5} & 0.148 \end{bmatrix}$$

$$\mathbf{C}_s = \begin{bmatrix} 0.0016 & 0 & -0.001 & 0 & 0 & 0 \\ 0 & 0.0047 & 0 & 0 & 0 & 0 \\ -0.001 & 0 & 6.54\times10^{-4} & 0 & 0 & 0 \\ 0 & 0 & 0 & 0.0130 & 0 & 0.0095 \\ 0 & 0 & 0 & 0 & 0.0015 & 0 \\ 0 & 0 & 0 & 0.0083 & 0 & 0.148 \end{bmatrix}$$

$$\boldsymbol{\xi} = \begin{bmatrix} 0.0022 & 2.0777\times10^{-5} & 0.0047 & 0.0124 & 0.1486 & 0.0015 \end{bmatrix}$$

$$\boldsymbol{\Gamma} = \begin{bmatrix} 0.8449 & 0.5350 & 0 & 0 & 0 & 0 \\ 0 & 0 & 1 & 0 & 0 & 0 \\ -0.5350 & 0.8449 & 0 & 0 & 0 & 0 \\ 0 & 0 & 0 & 0.9981 & 0.0699 & 0 \\ 0 & 0 & 0 & 0 & 0 & 1 \\ 0 & 0 & 0 & -0.1113 & 0.9976 & 0 \end{bmatrix}$$

V. CONCLUSION

In this paper, a theoretical characterization of the primary mobility of the dual-continuum-joint translator is presented.

Cosserat rod theory is first used to establish a kinestatic model of the translator as a multi-rod system with multiple boundary conditions. The compliance matrices of the translator are then calculated and the primary mobility is quantified using screw theory.

Two simulation cases with different external forces exerted on the DJ's end disk of the translator were investigated. The simulation results show that the continuum joints (the PJ and the DJ) bend into the shapes close to circular arcs. The

maximum deviations from the calculated shapes to circular arcs are 0.016 mm. Bending angles of the PJ and the DJ are similar due to the coupling between them. The maximal rotation angle of the DJ's end disk is less than 0.889°, indicating a translational motion outputs.

The calculated compliance matrices also indicate that a rotation mobility along the z axis of the translator, which is not intended. Twisting resistant components should hence be arranged to minimize this possible twist so that the primary mobility of the translator is sole translation.

REFERENCES

[1] I. D. Walker, "Continuous Backbone "Continuum" Robot Manipulators," *ISRN Robotics,* vol. 2013, No.726506, pp. 1-19, 2013.

[2] S. Hirose, *Biologically Inspired Robots, Snake-Like Locomotors and Manipulators*. Oxford: Oxford University Press, 1993.

[3] J. Peirs, D. Reynaerts, H. Van Brussel, G. De Gersem, and H.-W. Tang, "Design of an Advanced Tool Guiding System for Robotic Surgery," in *IEEE International Conference on Robotics and Automation (ICRA)*, Taipei, Taiwan, 2003, pp. 2651-2656.

[4] N. Simaan, R. H. Taylor, and P. Flint, "A Dexterous System for Laryngeal Surgery," in *IEEE International Conference on Robotics and Automation (ICRA)*, New Orleans, LA, 2004, pp. 351-357.

[5] J. Burgner-Kahrs, D. C. Rucker, and H. Choset, "Continuum Robots for Medical Applications: A Survey," *IEEE Transactions on Robotics,* vol. 31, No.6, pp. 1261-1280, Dec 2015.

[6] P. Dario, M. C. Carrozza, and A. Pietrabissa, "Development and In Vitro Testing of a Miniature Robotic System for Computer-Assisted Colonoscopy," *Computer Aided Surgery,* vol. 4, No.1, pp. 1-14, 1999.

[7] S. Liu, Z. Yang, Z. Zhu, L. Han, X. Zhu, and K. Xu, "Development of a Dexterous Continuum Manipulator for Exploration and Inspection in Confined Spaces," *Industrial Robot: An International Journal,* vol. 43, No.3, pp. 284-295, 2016.

[8] K. Suzumori, S. Iikura, and H. Tanaka, "Development of Flexible Microactuator and Its Applications to Robotic Mechanisms," in *IEEE International Conference on Robotics and Automation (ICRA)*, Sacramento, CA, USA, 1991, pp. 1622-1627.

[9] G. Immega and K. Antonelli, "The KSI Tentacle Manipulator," in *IEEE International Conference on Robotics and Automation (ICRA)*, Nagoya, Aichi, Japan, 1995, pp. 3149-3154.

[10] W. McMahan, V. Chitrakaran, M. Csencsits, D. M. Dawson, I. D. Walker, B. A. Jones, M. Pritts, D. Dienno, M. Grissom, and C. D. Rahn, "Field Trials and Testing of the OctArm Continuum Manipulator," in *IEEE International Conference on Advanced Robotics (ICAR)*, Orlando, FL, USA, 2006, pp. 2336-2341.

[11] C. E. Bryson and D. C. Rucker, "Toward Parallel Continuum Manipulators," in *IEEE International Conference on Robotics and Automation (ICRA)*, Hong Kong, China, 2014, pp. 778-785.

[12] Z. Yang, X. Zhu, and K. Xu, "Continuum Delta Robot: a Novel Translational Parallel Robot with Continuum Joints," in *IEEE/ASME International Conference on Advanced Intelligent Mechatronics (AIM)*, Auckland, New Zealand, 2018, pp. 748-755.

[13] J. Yu, S. Bi, G. Zong, J. S. Dai, and X.-j. Liu, "Mobility Characteristics of a Flexure-Based Compliant Manipulator with Three Legs," in *IEEE/RSJ International Conference on Intelligent Robots and Systems (IROS)*, Beijing, China, 2006, pp. 1076-1081.

[14] J. Till, C. E. Bryson, S. Chung, A. Orekhov, and D. C. Rucker, "Efficient Computation of Multiple Coupled Cosserat Rod Models for Real-Time Simulation and Control of Parallel Continuum Manipulators," in *IEEE International Conference on Robotics and Automation (ICRA)*, Seattle, Washington, 2015, pp. 5067-5074.

[15] D. C. Rucker and R. J. Webster, "Computing Jacobians and Compliance Matrices for Externally Loaded Continuum Robots," in *IEEE International Conference on Robotics and Automation (ICRA)*, Shanghai, China, 2011, pp. 945-950.

[16] A. L. Orekhov, V. A. Aloi, and D. C. Rucker, "Modeling Parallel Continuum Robots with General Intermediate Constraints," in *IEEE International Conference on Robotics and Automation (ICRA)*, Singapore, 2017, pp. 6142-6149.

[17] S. S. Antman, *Nonlinear Problems of Elasticity*, 2nd ed. vol. 107. New York: Springer, 2005.

[18] K. Xu and N. Simaan, "Analytic Formulation for the Kinematics, Statics and Shape Restoration of Multibackbone Continuum Robots via Elliptic Integrals," *Journal of Mechanisms and Robotics,* vol. 2, No.011006, pp. 1-13, Feb 2010.